Title: Cellular characterization of the peritumoral brain zone of glioblastomas: heterogenous nature and clinical relevance.

Running title: Deciphering the infiltrative ecosystem of glioblastomas.

Olaya de Dios[1], Juan Romero[2], María de los Ángeles Ramírez-González[1], Beatriz Herranz[3], Alicia Avis[1], Ana Ramos, Juan Manuel Sepúlveda-Sánchez[4], Ricardo Gargini[4], Bárbara Meléndez[5], Pedro González[6], Luis Jiménez-Roldán[6], Guillermo García-Posadas[6], Aurelio Hernández-Laín[4], Ángel Pérez-Núñez[*6], Pilar Sánchez-Gómez[*1]

[1] NeuroOncology Unit, Chronic Disease Department (UFIEC), Instituto de Salud Carlos III, Madrid, Spain.
[2] Department of Radiology, Hospital Universitario 12 de Octubre Madrid, Spain.
[3] Medical School, Universidad Francisco de Vitoria, Madrid, Spain
[4] Neurooncology Unit, Instituto de Investigaciones Biomédicas I+12, Hospital 12 de Octubre, Madrid, Spain.
[5] Molecular Pathology Research Unit. Hospital Virgen de la Salud, Toledo, Spain
[6] Department of Neurosurgery, Instituto de Investigaciones Biomédicas I+12, Hospital 12 de Octubre, Madrid, Spain.

* Corresponding author

CORRESPONDING AUTHOR E-MAIL ADDRESS:

Pilar Sanchez-Gomez, psanchezg@isciii.es

Angel Pérez-Núñez, apnunez@salud.madrid.org

Abstract

Background: Glioblastoma (GB) is a highly aggressive cancer with nearly 100% recurrence, even after removal of all contrast-enhancing (CE) disease. This is primarily due to the persistence of residual tumor cells in the peritumoral brain zone (PBZ), which can repopulate the GB after treatment. The aim of this study was to characterize the degree of neoplastic infiltration and the tumor microenvironment (TME) in the periphery of these aggressive tumors.

Methods: We generated a prospective collection of radiologically guided biopsies from GB patients where we performed a comprehensive immunohistochemical analysis. We also integrated publicly available single-cell RNA sequencing datasets from human brains and gliomas to create an atlas of major cell types and select specific markers of immune cells, astrocytes,

oligodendrocytes, and vascular cells. This gene panel was used to characterize the cellular content of biopsies from various regions, including CE tumor, non-CE tumor, edema, and radiologically normal tissue.

Results: High levels of GB infiltration were found in non-CE regions, which explains the clinical benefit of extending surgery to these areas. However, tumorigenic signs were also found in areas that were associated with vasculogenic edema. The analysis of the biopsies revealed inter-tumor heterogeneity in the PBZ, with variations in cellular composition linked to tumor infiltration, patient age, and sex. Additionally, we identified cellular features, both in the tumor core and the periphery, that were distinctly associated with the prognosis of the patients depending on the extent of resection.

Conclusions: Our results support the notion that non-CE tumor areas are infiltrated by GB cells, although they expand as well to extra-tumoral regions. Moreover, our characterization of the cellular profile of the PBZ suggest key targets for GB progression, which might be different in patients receiving complete or uncomplete resections of the CE disease, or in female vs male patients.

Keywords: Glioblastoma, Peritumoral brain zone, Extent of resection, Tumor infiltration, Tumor microenvironment, sex-related differences.

Funding: This work was supported in part by Ministerio de Ciencia, Innovación y Universidades and FEDER funds: PI21/01406 (J.M.S.), PI22/01171 (R.G.), PI21/01168 (A.P.N.), PI21CIII/00002 (P.S.G.), TED2021-132318B-I00 (P.S.G.), P2022/BMD-7344 (P.S.G.), Miguel Servet Contract CP21/00116 (R.G.); by the American Brain Tumor Association Research Collaboration Grant ARC2300007 (P.S.G.) and by the ReachGLIO project, under the framework of the ERA-NET TRANSCAN-3 initiative JTC 2022 call (funded by the Institute of Health Carlos III (ISCIII) (AC23CIII_1-00003), and the Scientific Foundation of the Spanish Association Against Cancer (TRNSC235658SANC)).

Introduction

Diffuse gliomas are histologically classified as low and intermediate-grade gliomas (grades 2 and 3) (herein called Lower-Grade Gliomas, LGG), or high-grade gliomas (glioblastomas (GBs) and grade 4 astrocytomas). The 2016 WHO classification of tumors of the CNS incorporated molecular data to the criteria required for diagnosis, particularly regarding the status of *IDH* (*isocitrate dehydrogenase*), whose mutations accumulate in LGGs and in grade 4 astrocytomas and is absent in GBs. The latter is the most common and lethal tumor of the central nervous system (CNS) with 5-year survival rates of only 5% [1]. Magnetic resonance imaging (MRI) is the gold standard technique to diagnose and characterize gliomas. They are shown as intra-axial infiltrative lesions, with ill-defined margins with the neighboring brain. The typical picture of a GB is that of a contrast-enhancing (CE) lesion, sometimes heterogeneous due to intra-tumoral necrosis, cysts or hemorrhage, surrounded by a hyper intense area in T2-weighted fluid-attenuated inversion recovery (FLAIR) sequences.

Although gliomas do not metastasize, they colonize the brain parenchyma, even in the less aggressive LGG forms. Although invasiveness is not a specific attribute of the deadliest GB, it drives treatment resistance in these tumors. This feature explains why, even after complete resection of the CE area, which is followed by radiotherapy targeting the tumor bed and systemic treatment with temozolomide (TMZ), GB invariably recurs, commonly at the edge of the resection cavity [2]. Recent studies suggest that infiltrative GBM regions can be detected using FLAIR sequences, where the non-CE tumor appears as mild-to-high signal intensity lesions [3, 4]. However, distinguishing non-CE tumor from edema, also characterized by high FLAIR signals, remains challenging and largely depends on subjective radiological criteria. Furthermore, a subset of GB cases lacks detectable non-CE regions, indicating that infiltrative tumor areas are not always visible on conventional MRI. The concept of supratotal resections has gain traction in recent years. This approach aims to remove as much tumor as possible, including both CE and non-CE regions, provided it can be done safely without causing significant neurological sequelae. Several studies have reported a significant increase in overall survival for GB patients, averaging 6 months, an outcome that no oncological treatment has matched thus far [5, 6]. In light of this, new RANO criteria has been proposed to classify the extent of surgical resection [7], and clinical trials are underway to validate the survival benefits of these extended resections [8].

The above findings underline the need to characterize the hyperintense FLAIR region, the so-called peritumoral brain zone (PBZ) in GB patients, which has been shown to content a mix of tumor cells, immune system cells, reactive astrocytes, and cells from the oligodendrocyte lineage, within a vascular context that differs significantly from that of the tumor core [9-12]. However, despite these advancements, there is a paucity of large-scale studies investigating the variances between distinct radiological regions (e.g., non-CE vs edema) or the existence of differences among various patient groups. Furthermore, none of these studies have correlated their findings with disease progression. Here we prospectively generated a cohort of radiologically-noted biopsies from the enhancing nodule and the periphery, and we also determined the extent of resection in all the patients included in the study. We observed that the presence of even residual CE disease after surgery has a strong negative impact on the overall survival of GB patients. In order to measure the amount of GB infiltration in the collected samples, we performed an immunohistochemical (IHC) analysis of proliferative cells. Moreover, we used publicly available single-cell RNA sequencing (sc-RNAseq) data to select genes specific for the different cell types in the brain microenvironment. The IHC study confirmed that areas of non-CE tumor contain an important number of proliferating cells and their cell density is similar to that of the tumor core. However, we also found pathological features in areas classified as edema or even in regions with no radiological alterations, particularly in female and elderly patients. Furthermore, the application of unsupervised clustering to the differential gene expression analysis enabled the separation of the most pathogenic samples, which included CE and non-CE tumor biopsies, based on the enrichment of proliferative markers and the pronounced absence of normal endothelial and oligodendrocyte expression. Notably, different cellular features in the tumor core and in the PBZ, mainly those associated with immune cells and astrocytes, were associated with GB prognosis, showing different trends in patients receiving complete or uncomplete resection of the CE tumor. Moreover, we observed important differences in the cellular features of the PBZ in female and male patients, associated with distinct prognostic impact. Our results suggest that tumor infiltration depend on the phenotype of the tumor core, but is also age and sex-dependent. Moreover, therapeutic strategies aiming at the residual GB disease should carefully consider the extent of resection and the subgroup of patients.

Methods

The workflow followed in this manuscript is illustrated in Table S1A.

Human samples.

We performed a prospective study with patients diagnosed of GB at Hospital 12 de Octubre, in accordance with the Declaration of Helsinki and obtained the approval of the local ethics committee, Catania 1 (CEI_21/480). All the patients involved gave their written informed consent. Inclusion criteria were: (i) histologically proven GBM, IDH-wt; (ii) age > 18 years. Pre-operative MRI were used to determine tumor volume and location, and to select the different regions of the tumors to be biopsied to generate the cohort of samples. This information was used by the neurosurgeons as a guide to select the biopsies taken, always trying to perform the most extended and safest resection of the patient´s tumor. Screenshots were taken during surgery to confirm the location of the samples. At least two radiologists reviewed the surgical images and categorized the biopsies as CE-tumor (CE), non-CE tumor (non-CE), vasogenic Edema (E), or radiologically-normal (N) regions. Post-operative MRI (obtained ≤ 72 h after surgery whenever possible) were used by radiologists to categorize the extent of resection of each patient. Histopathological examination confirmed the presence of IDH-wildtype and gave a first assessment of tumor infiltration into the peripheral zone. The list of patients and samples collected is detailed in Supp. Table S1B.

RNA Extraction and Quantitative PCR.

Total RNA from the human samples was extracted using the TRIzol reagent (Invitrogen) following the protocol detailed in Table S1D. The equivalent amounts (1 µg) of purified RNA were reverse transcribed using PrimeScript RT Reagent Kit (Takara). Quantitative real-time PCR was performed using the LightCycler 480 (Roche Diagnostics) with the SYBR Premix (TB Green® Premix Ex Taq™ II, Takara) and gene-specific primers (Table S1C). To determine the most suitable reference gene for normalization, *GAPDH*, *HPRT*, and *RPII* were tested as candidate housekeeping genes. After assessing the consistency of expression across the three reference genes, *GAPDH* was selected for normalization. All reactions were performed in technical duplicates, and no-template controls (NTCs) were included. Relative gene expression was calculated using the ΔΔCt method and normalized to *GAPDH*.

Immunohistochemical (IHC) staining and quantification. MIB-1 IHC staining (Table S1C) were performed on brain tissue sections from the murine model or from patient´s tumors that had been previously fixed in 4% formalin, paraffin-embedded, and sectioned onto slides of 4 µm thickness. Before DAB, slides were dewaxed and stained with hematoxylin and eosin to examine the sample. For the chromogenic detection, the slides were prior preheated for 30 minutes at 65°C and the BOND RXm automated advanced staining system (Leica Biosystems) programmed with the specific protocol according to the staining type was used (Table S1E).

The chromogenic slides were scanned using the Hamamatsu NanoZoomer-SQ microscope slide digitizer (C13140-01). QuPath software was used for the quantification with setting of the positive-cell detection method by calculating the percentage of positive cells in comparison to negative cells within a consistently defined area for each stain. The specific code and parameters used for quantification of each stain are detailed in Table S1F.

In silico studies.

scRNA-seq datasets analysis. For this study, we utilized our previously published integrated human single-cell transcriptomic atlas, which was generated by integrating publicly available scRNA-seq datasets from normal brain, IDHmut gliomas, and GBMs, as described previously [13] (Table S1C). Moreover, to validate the key genes in the tumor periphery the already processed RDS files [14] were downloaded from the respective public repositories. Data processing and analysis that followed were also conducted using the Seurat package v4.3.0.

Differential gene expression analysis. Differentially expressed genes (DEGs) were determined with the Seurat functions *FindAllMarkers* and *FindMarkers*. We use *FindAllMarkers* to find markers differentially expressed in each cluster by comparing them to all the others, which we refer to as Cell-Type Specific Markers, while we use FindMarkers to find markers between two different conditions in the same cluster. For computing DEGs, all genes provided were expressed in at least 25% of cells in either of the two populations compared and the expression difference on a natural log scale was at least 0.25.

Key Genes Analysis. To identify cancer-associated specific to the main glioma subtypes, two different types of analysis were performed. The workflow following for this analysis was the following (Supp. Fig. 1).

Analysis 1. Identification of Key Genes from DEGs. This analysis integrates 4 different list of DEGs to identify key genes associated with glioma and specific cell types:

(1) **Cell-Type Specific Markers in the Integrated Single-Cell Atlas.** DEGs that are markers of each cell type within the integrated single-cell atlas (S2.A1). The following parameter settings were used for defining markers across clusters: ptc.2 ≤ 0.1 for most of the clusters, ptc.2<0.2 for Astrocytes-C10, and ptc.2 < 0.3 for endothelium, mural cells, and neurons.

(2) **DEGs in Homeostasis vs. LGG Patients.** DEGs in homeostasis versus LGG patients (S2.A2) within each specific cluster (parameter settings: avg_log2FC =<-1).

(3) **DEGs in Homeostasis vs. Newly Diagnosed GBM Patients.** DEGs in homeostasis versus newly diagnosed GBM patients (S2.A3) within each specific cluster (parameter settings: avg_log2FC =<-1).

(4) **DEGs in Homeostasis vs. Recurrent GBM Patients.** DEGs in homeostasis versus newly recurrent GBM patients (S2.A4) within each specific cluster (parameter settings: avg_log2FC =<-1).

The overlapping genes among these three lists in each specific cell type (S2.A5) were defined as key gene candidates (Table S1F), representing shared molecular alterations across conditions and specific to each cell type.

We further evaluated the key gene candidates by comparing GTEx Brain-Cortex and GTEx Brain-Frontal Cortex versus TCGA Brain Lower-Grade Glioma (LGG) and Glioblastoma Multiforme (GBM) datasets (Table S1F – List 1). To assess significant expression differences, we applied Welch's t-test (TCGA vs. GTEx) [15], identifying the most differentially expressed genes between normal brain tissue and glioma samples (Table S1F – List 2).

Analysis 2. Identification of key genes from conservative markers. In this analysis we performed a Venn Diagram-based comparison between the significative conservative markers in the homeostasis condition and glioma patient samples, alongside cell-type specific markers identified in the Integrated Single-Cell Atlas (parameter settings: ptc.2 ≤ 0.1). This approach was applied as an alternative method in cases where Analysis 1 did not yield strong markers for certain cell types. It allowed us to extract key markers for endothelial cells and oligodendrocytes.

Finally, from the lists of candidate genes, we visualized their expression in the integrated single-cell atlas and the Core/Peripheral database to select the most cell-type-specific genes (S3)

Kaplan-Meier Plots. To assess the prognostic value of the expression of the markers in GBM we used the *The Human Protein Atlas* web tool [16] (proteinatlas.org). RNA sequencing (RNAseq) data came from the Cancer Genome Atlas (TCGA). The best cutoff algorithm was used to divide bladder cancer patients into high- or low-expression groups. The best cutoff is based on the FPKM value of each gene, patients were classified into two groups and association between prognosis (survival) and gene expression (FPKM) was examined. The best expression cut-off refers the FPKM value that yields maximal difference with regard to survival between the two groups at the lowest log-rank P-value.

Cell Type RNA expression. To confirm cell-type-specific genes of the markers we employ the *The Human Protein Atlas* web tool [16]. The RNA specificity category is based on mRNA expression levels in the analyzed cell types based on scRNA-seq data from normal tissues. The RNA data was used to cluster genes according to their expression across single cell types. Clusters contain genes that have similar expression patterns, and each cluster has been manually annotated to describe common features in terms of function and specificity.

Molecular characterization of the tumors.

Biopsies were stored in RNAlater (frozen samples) or in PFA and (formalin-fixed paraffin-embedded (FFPE) samples) (workflow is shown in Supp. Fig. 1A). DNA was extracted from selected FFPE tumor tissues using the QIAamp DNA FFPE Tissue Kit (Qiagen) following manufacturer's instructions and was quantified using Qubit 2.0 Fluorometer (Thermo Fisher Scientific). We used a custom Ampliseq (PCR-based) gene-targeted next-generation sequencing (NGS) panel that analyzes 30 genes that were previously demonstrated to be frequently mutated in gliomas. A second custom Ampliseq gene-targeted NGS panel used for routine glioma diagnosis was also applied to the samples in order to complete and validate the findings. This panel allowed to reanalyze some of the genes and added the information on hotspot mutations of the TERT promoter, together with the 1p/19q codeletion, EGFR, EGFRviii, and PDGFRA amplifications, as well as CDKN2A and PTEN homozygous deletions using a BELAC ISO 15189 accredited protocol [17]. MGMT methylation status was assessed with pyrosequencing method.

RNA Extraction and Quantitative PCR.

Total RNA was extracted using the TRIZOL method. Equivalent amounts (1 µg) of purified RNA were reverse transcribed using PrimeScript RT Reagent Kit (Takara). Quantitative real-time PCR

was performed using the LightCycler 480 (Roche Diagnostics) with the SYBR Premix (TB Green® Premix Ex Taq™ II, Takara) and gene-specific primers (Supp. Table 1B). Relative gene expression was calculated using the ΔΔCt method and normalized to *GAPDH*.

Immunohistochemical (IHC) staining and quantification.

IHC staining with the MIB-1 antibody was performed on 4 µm brain tissue sections from patient´s tumors. The slides were prior preheated for 30 minutes at 65°C and the BOND RXm automated advanced staining system (Leica Biosystems) programmed with a specific protocol. The chromogenic slides were scanned using the Hamamatsu NanoZoomer-SQ microscope slide digitizer (C13140-01). QuPath software was used for the quantification of the percentage of positive cells in comparison to negative cells within a consistently defined area for each stain. In contrast, for CD68, CD206, and NKG2C stains, the pixel classification method was applied. Cell density in each area was calculated by the number of nuclei.

Single-cell RNA-seq datasets analysis.

The generation of the integrated single-cell transcriptomic atlas was already described in a recent manuscript [13]. In summary, we downloaded different scRNAseq databases available in public repositories of normal brain [18], IDHmut gliomas, and GBMs [19]. Subsequent data processing and analysis were performed using the Seurat package v4.3.0. For the analysis, the two IDHmut samples were selected, and in the case of GBMs, the three cases of newly diagnosed and recurrent GBM with the highest number of counts were chosen (Table S1C). Integration and batch-corrected dimensionality reduction were performed using Harmony (20) correcting for sample type. Cell types were identified using scCATCH (Single-Cell Cluster-Assisted Annotation Toolkit for Cellular Heterogeneity) [20] and confirmed by canonical markers described in a previous study [21] (Supp. Fig. 1A).

Statistics.

All statistical analyses were performed using R (v.4x.) and GraphPad Prism (10.1.2). Data normality was assessed using the Shapiro-Wilk test. As most datasets did not follow a normal distribution, non-parametric tests were applied. For comparisons between two groups, the Wilcoxon rank-sum test (Mann-Whitney U test) was used. For comparisons across multiple groups, the Kruskal-Wallis test followed by Dunn's post hoc test was performed. Correlations between variables were assessed using Spearman's correlation coefficient (ρ). Kaplan-Meier survival analysis was

conducted to evaluate overall survival (OS), with differences between groups assessed using the log-rank (Mantel-Cox) test. All statistical tests were two-tailed, and a p-value ≤ 0.05 was considered statistically significant.

Results

Analysis of GB infiltration by immunohistochemical analysis.

Forty-five patients were enrolled in the study (Fig. 1A, Supp. Fig. 2A). The extent of resection was categorized as: (i) supratotal (class 1), beyond CE tumor borders; (ii) complete (class 2a), removal of all CE tumor; (iii) neartotal (class 2b), less than 1 cm3 of residual CE tumor; (iv) subtotal (class 3a), between 1-5 cm3 of residual CE tumor; (v) partial (class 3b), >5 cm3 residual CE tumor; (v) biopsy (class 4), no tumor reduction (Fig. 1B). In our cohort, the presence of even small areas of CE tumor after surgery had a strong impact in the prognosis of the patients, and no differences were observed between patients that have received neartotal or subtotal surgeries (Fig. 1C). For that reason and to increase the statistical power of our correlation studies we clustered the patients as those receiving a gross total resection (GTR) of the CE tumor (suptratotal and complete) and those receiving a non-GTR (neartotal, subtotal, partial and biopsy) (Supp. Fig. 2B). The methylation of the O-6-methylguanine-DNA methyltransferase promoter (MGMTp) was associated with better, but not significant, prognosis, particularly in patients receiving GTR (Supp. Fig. 3A). Although a worse prognosis has been attributed to elderly GB patients (≥65yo) [22], it was not the case in our cohort, although there was an accumulation of unmethylated MGMTp tumors among younger patients that could explain this result (Supp. Fig. 2B). Interestingly, we did observe a worse prognosis (albeit not significant) when comparing elderly to young patients among the non-GTR group (Supp. Fig. 2B). Finally, female patients showed a shorter survival, which doesn´t seem to be affected by the extent of resection, although it could be explained by a higher accumulation of methylated MGMTp tumors among male patients (Supp. Fig. 2C).

We collected 165 biopsies from the different radiological regions (Fig. 1D). One part of the samples was embedded in paraffin and the number of Ki-67/MIB-1+ cells was quantified by IHC analysis (Fig. 1E). As expected, the biopsies from the CE tumor showed the highest cell density and proliferating index, although non-CE samples also showed significantly higher levels of both parameters in comparison with other peritumoral biopsies (E and N). Interestingly, there was no difference in terms of cellularity between CE and non-CE biopsies (Fig. 2A). High MIB-1 labelling index and high cellularity were also observed in several extra-tumoral (edema and normal) biopsies (Fig. 2A) and this event was more frequent among female (Fig. 2B) and elderly (Fig. 2C) patients. Cell density, by contrast, was higher among the intra-tumoral biopsies from male (Fig. 2B) and younger (Fig. 2C) patients.

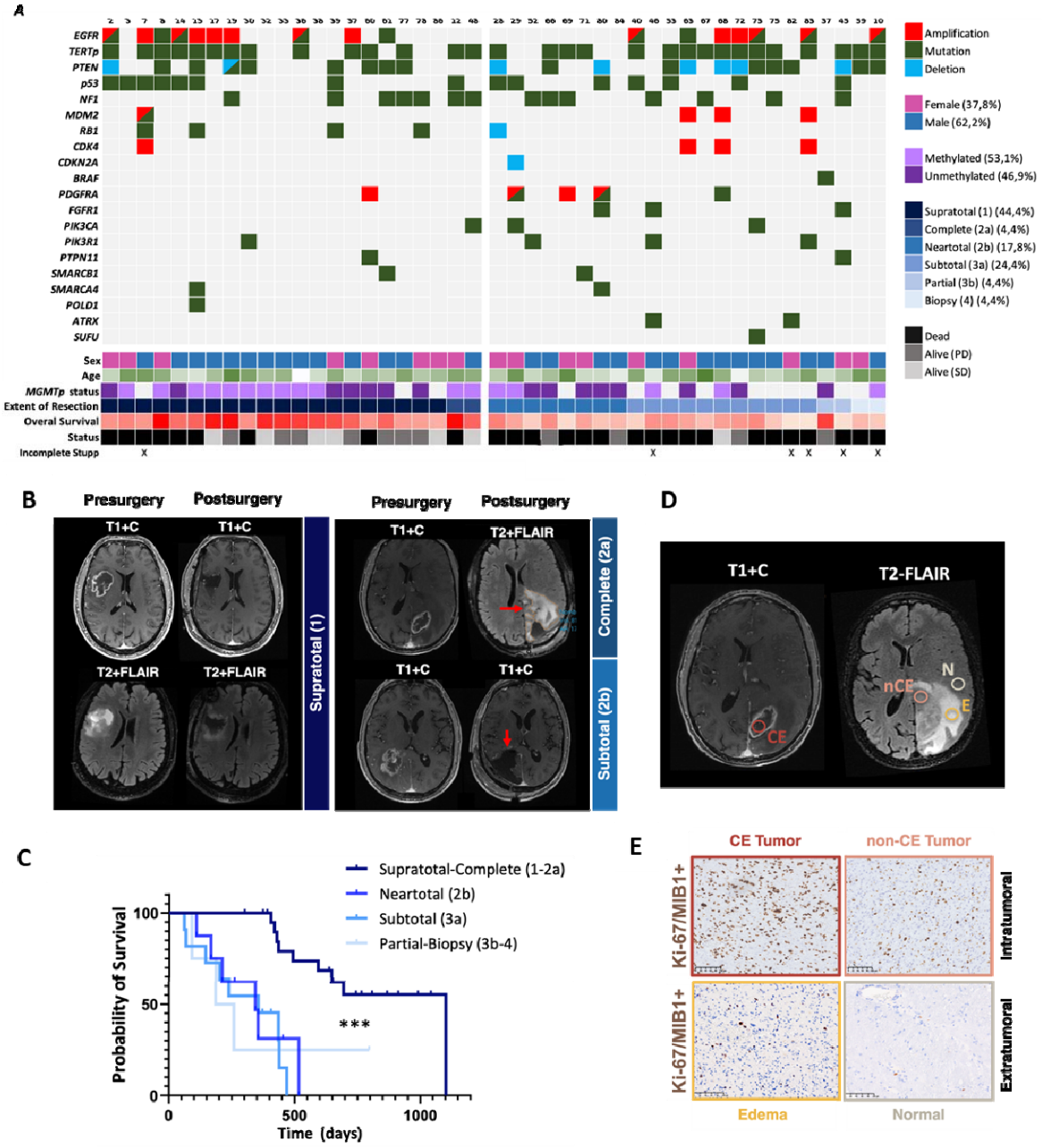

Figure 1. Characteristics of the patients and the biopsies analyzed in this study. A) Oncoplot of genetic variants in all GB tumors included in the study. The main clinical features are shown color coded in the bottom. **B)** MRI images (T1 sequence + contrast, T1+C; T2 FLAIR sequence, FLAIR) of three representative patients. The images were obtained before and after surgery. The extent of resection of each patient is lablelled on the right. The red arrows point towards areas of residual tumor observed in FLAIR (in a complete resection case) or in T1+C (in a subtotal resection case). **C)** Kaplan-Meier survival curve analysis of patients in the cohort based on the extent of resection. **D)** Representative T1+C and T2-FLAIR images of one of the patients enrolled in the study. The location of radiologically-guided biopsies are marked with colored circles. **E)** Representative

images of the immunohistochemical (IHC) staining using the MIB1 antibody in different radiological regions. PD: progressive disease, SD: stable disease. Scale bar (E): 100mm. *** P≤0.001

As an alternative to this quantitative approach, we classified the biopsies based on the level of tumor infiltration, either based on the MIB-1 index or cell density, as: (i) no infiltrated (NO), those below the median level of the extra-tumoral samples; (ii) low infiltrated (LOW), those in the second quartile; (iii) high infiltrated (HIGH), those above the 75% level among the extra-tumoral values. This qualitive approach confirmed the high degree of tumor infiltration in non-CE areas, but also in several edema and normal biopsies (Fig. 2D). Interestingly, there was not a direct correlation between the MIB-1 labelling index and the cell density of the samples, with some extra-tumoral biopsies showing high MIB-1 labelling index, even though the cell density was not clearly elevated, and some other having the opposite trend (Fig. 2E). We then classified the tumors as overall infiltrative (when we detected high or low % of MIB-1+ cells or high/low numbers of cell density in one or more extra-tumoral biopsies) or non-infiltrative (those patients from whom we collected at least two extra-tumoral biopsies without signs of tumor infiltration). We observed a significant accumulation of female and elderly patients among the infiltrated tumors, but only when the classification was made based on MIB1 labelling index (Fig. 2F). Interestingly, only the presence of higher cellularity in the extra-tumoral biopsies impacted negatively on the prognosis of the patients (Fig. 2F), though there was a significant accumulation of non-GTR among this group of patients. Overall, the IHC results reinforce the relevance of extending the surgical margins beyond the CE limits to areas of non-CE tumor. However, they also suggest that surgery should even include, whenever feasible, adjacent regions associated with vasculogenic edema or those showing no FLAIR alterations. Moreover, our findings allow us to hypothesize that high cellularity at the tumor margin could difficult the delimitation of the enhancing tumor border by neurosurgeons, even if using the 5-aminolevulinic acid (5-ALA) reagent, leading to higher volume of CE residual disease.

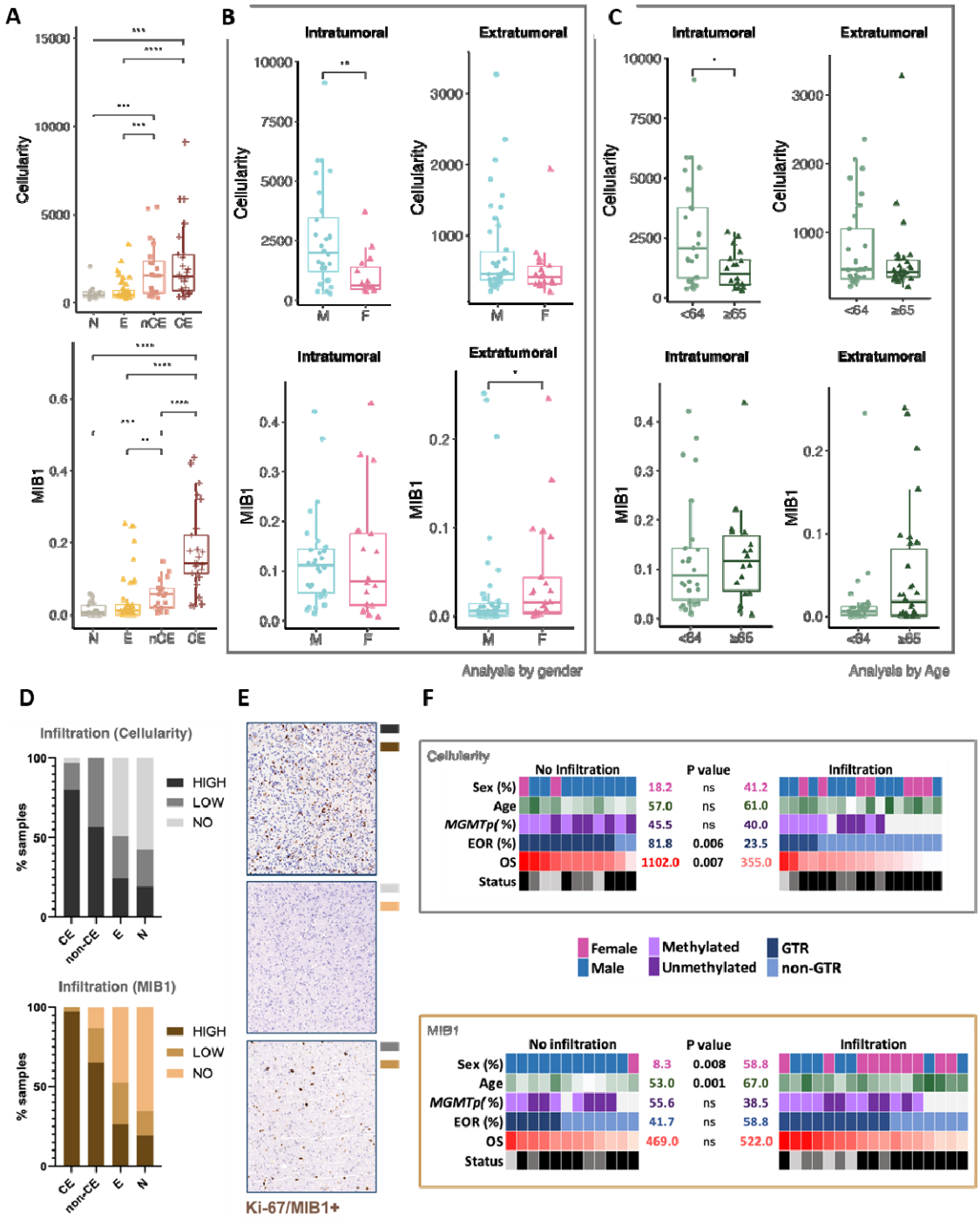

Figure 2. Immunohistochemical (IHC) analysis of the samples. A) Quantification of cell density (up), and MIB1 labeling index (down) in the different categories of biopsies. **B-C)** Quantification of cell density (up), and MIB1 labeling index (down) in intra and extra-tumoral biopsies from male and female **(B)** and young and old **(C)** GB patients. **D)** Percentage of samples categorized as HIGH, LOW or NO infiltrated in the different radiological categories. They were measured by cell density (up) or % of MIB1+ cells (down). **E)** Representative images of MIB1 IHC staining in the extra-tumoral (Edema + Normal) regions of different patients. The category of tumor infiltration by MIB-

1 index (blue) or cell density (green) in shown on the right. F) The tables show the main clinical features of patients showing signs of tumor infiltration or not. The classification was based on the presence of extratumoral samples categorized as infiltrated (High or Low) based on cell density (up) or MIB1 labelling index (down). The table in the middle depicts the percentage of female, *MGMTp* methylated or GTR patients in the two groups. The P value was estimated by the Fishers test. It also shows the median age (P value by Mann Whitney test) and the median overall survival (OS) (P value by Log-rank (Mantel-Cox) test). ns, non-significant, * P≤0.05,** P≤0.01, *** P≤0.001, **** P≤0.0001.

Molecular and cellular analysis of the cohort of biopsies.

The tumor microenvironment (TME) at the periphery of GB tumors is very different from that of the bulk. The periphery largely comprises normal brain tissue, whereas the bulk is characterized by hypoxic, necrotic, and angiogenic regions, suggesting distinct fate-choice pressures for tumor cells in these two areas. Here, to better characterize the TME of GBs we decided to select specific genes from each cell type and then measure their expression in our cohort of biopsies, as an indication of their cellular phenotype. We also included few samples from radiologically-normal regions of patients with non-GB diseases (one from a contusion case, one from a brain metastasis and one from a polymorphous low-grade neuroepithelial tumor case (PLNTY)). We used an integrated atlas generated based on publicly available scRNA-seq databases [13] (Supp. Fig. 4A-C) and we identified distinct clusters of immune cells (macrophages, microglia and T cells), astrocytic cells, oligodendrocytes and vascular cells (endothelial cells and pericytes) (Fig. 3A). We also found two clusters (glial and myeloid cells) that shared many genes overexpressed in gliomas, all of them related to cell proliferation (Figure 3A). After several refinement steps (see the Methods section), we selected a gene set specific for each cell type overexpressed in gliomas and confirmed that they show a differential expression in the different clusters and in normal brain and gliomas (Fig. 3B). We then measured the expression of the selected genes in our cohort of biopsies by means of qRT-PCR analysis and we analyzed the distribution of the different genes and gene sets (cellular "scores") in the different radiologically-guided biopsies. In agreement with the IHC studies, proliferative markers were highly expressed in CE and non-CE samples. Moreover, both tumorigenic regions could be distinguished from the rest of biopsies because they showed a strong decrease in the expression of oligodendrocytic genes (Fig. 3C). Non-CE biopsies showed an enrichment of astrocytic and T-cell markers, whereas CE samples showed a strong downregulation of normal endothelial cell genes. We also observed a reduced expression of myeloid-related genes

in normal biopsies compared to the other regions (Fig. 3C). Altogether, these results suggest that a different cellular phenotype is associated with the distinct radiological regions.

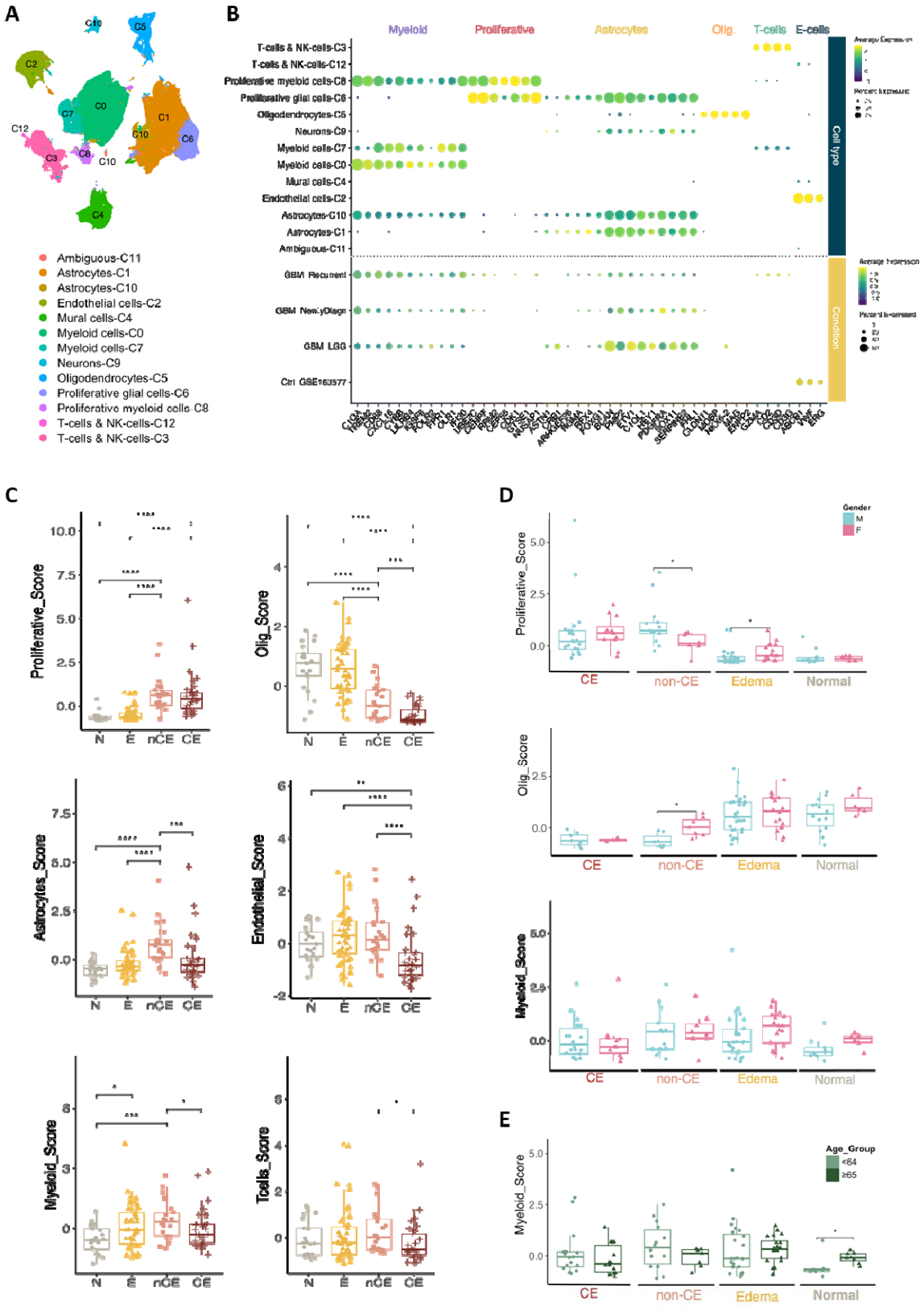
A
B
C
D
E
Ambiguous-C11
Astrocytes-C1
Astrocytes-C10
Endothelial cells-C2
Mural cells-C4
Myeloid cells-C0
Myeloid cells-C7
Neurons-C9
Oligodendrocytes-C5
Proliferative glial cells-C6
Proliferative myeloid cells-C8
T-cells & NK-cells-C12
T-cells & NK-cells-C3
Myeloid
Proliferative
Astrocytes
Olig.
T-cells
E-cells
Cell type
Condition
GBM Recurrent
GBM Newly Diagn
GBM LGG
Ctrl GSE163577
Proliferative_Score
Olig_Score
Astrocytes_Score
Endothelial_Score
Myeloid_Score
Tcells_Score
N
E
nCE
CE
Gender
M
F
non-CE
Edema
Normal
Age_Group
<64
≥65

Figure 3. Cellular characterization of the cohort. Correlation with age and gender. A) UMAP plot annotated according to each cell type of the integrated object (control and glioma scRNAseq databases). **B)** Dot plot showing the percentage and average expression of the selected markers in the different clusters of the integrated object and in the different conditions (control brain, low-grade gliomas (LGG), newly-diagnosed glioblastoma (ndGB) and recurrent glioblastoma (rGB). The dot.min value was set to 0.01, meaning only genes with expression levels above 1% are represented by a dot. **C)** Bar plots showing the log-transformed mean expression ("scores") of each cell type across different radiological regions: Normal (N), Edema (E), Non-Contrast Enhancing Tumor (nCE), and Contrast-Enhancing Tumor (CE). Statistical significance was assessed using the Kruskal-Wallis test. **D)** The graphs show the changes in the Proliferative, Oligodendrocyte and Myeloid scores between male (M) and female (F) patients in the different categories of samples. **E)** The graph shows the changes in the Myeloid score between young (<64 years) and old (≥65 years) patients in the different categories of samples. * P≤0.05, ** P≤0.01, *** P≤0.001, **** P≤0.0001.

We then compared samples from female and male patients and we observed striking differences in the proliferative and oligodendrocyte score in the non-CE and the edema category (Fig. 3D), with many genes showing a differential expression (Supp. Fig. 5A). They myeloid score was slightly higher in extra-tumoral biopsies from female GB patients (Fig. 3D), with many genes upregulated in both edema and normal biopsies (Supp. Fig. 5A). We also analyzed potential differences associated with age, but we could only observe a significant increase in the myeloid score of the normal biopsies from elderly patients (Fig. 3E), with few genes also showing a differential expression in nonCE, edema and normal samples (Supp. Fig. 5B). These findings suggest the existence of important cellular differences outside the enhancing tumor between male and female GB patients.

Unsupervised clustering of the samples.

The unsupervised clustering of the qRT-PCR expression data confirmed that the genes selected for the different cell types cluster together in the X axis (Fig. 4A). Regarding samples, we selected to group them in 5 clusters (Supp. Fig. 6) and we observed a high degree of similarity between CE and non-CE samples, which clustered together either in Cluster 3 (C3) and C4 (Fig. 4A-C). Both clusters were enriched in proliferative markers and showed lower expression of normal oligodendrocytes in comparison with the other three clusters. However, samples in C4 express higher levels of proliferative, astrocyte and endothelial cell markers. Most of the peritumoral samples were

distributed into three groups: C1, C2 and C5. C2 expresses higher levels of oligodendrocyte and T cell markers, and C5 shows higher levels of myeloid markers (Fig. 4A).

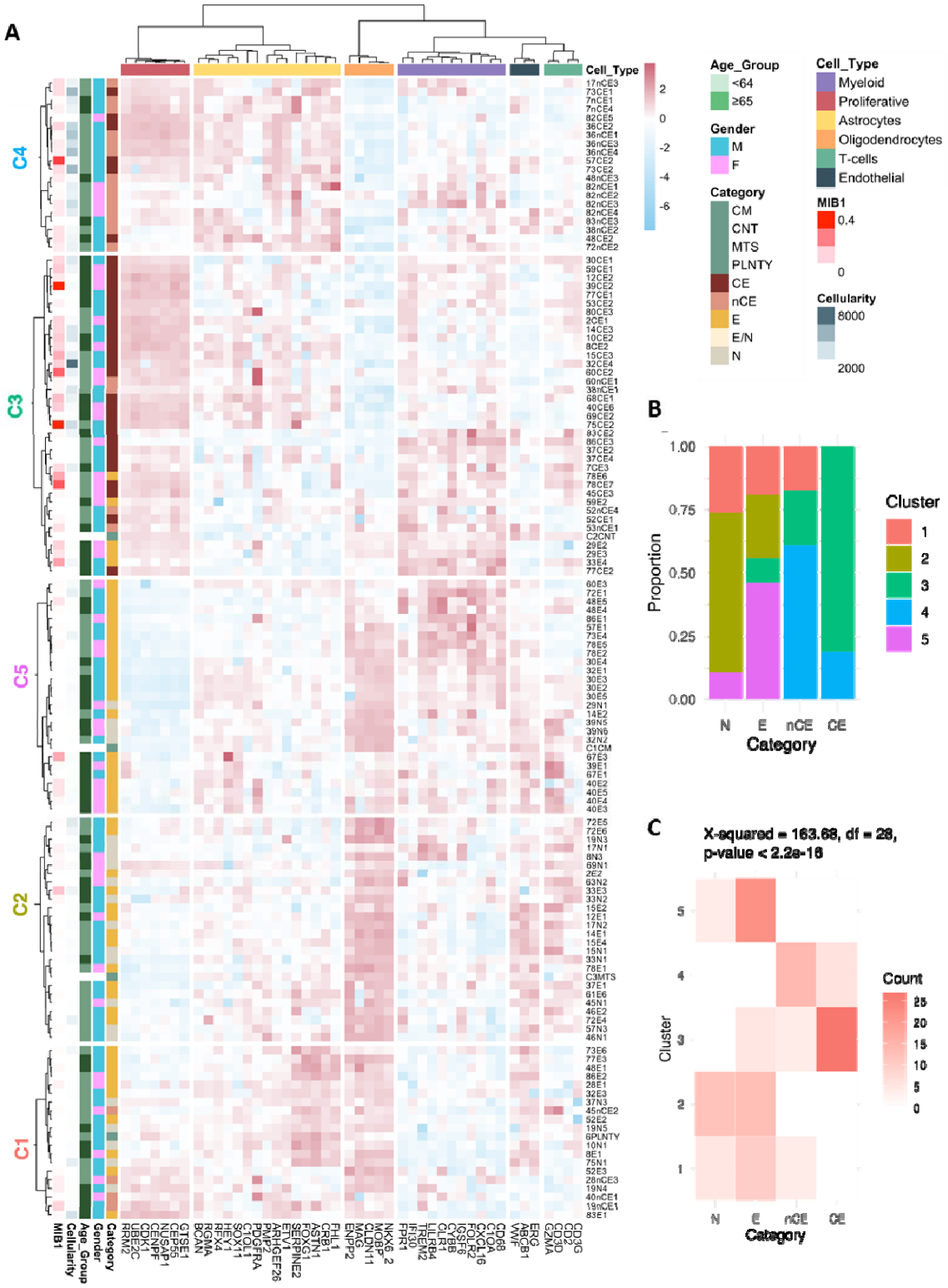

Figure 4. Classification of GBM biopsies using a cellular gene panel. A) The heatmap shows the unsupervised clustering of the different samples based on the expression of our panel of genes. **B)** Stacked bar plot showing the proportion of clusters (1–5) within each tissue category (N: Normal, E: Edema, nCE: Non-Contrast-Enhancing Tumor, CE: Contrast-Enhancing Tumor). **C)** Heatmap representing the distribution of tissue categories across clusters. Color intensity indicates cell counts per category. A chi-square test ($X^2 = 163.68$, df = 28, $p < 2.2e-16$) confirms a significant association between clusters and tissue types

Notably, some edema samples clustered together with CE and non-CE biopsies in C3 and they show high levels of MIB1% and cellularity, which suggest that they represent regions of tumor infiltration (Fig. 4A-C). Thus, we decided to analyze in detail the progression of patients with such edemas. In patient PTZ28 and PTZ29, the postsurgical MRI showed a small of CE residual tumor (neartotal resection) but in both cases, areas of edema with signs of tumor infiltration were also left behind (Fig. 5). Notably, tumor recurrence occurred very soon after surgery (6 and 3 months, respectively) in both areas, the one corresponding to the residual CE tumor and the one corresponding to the residual edema (Fig. 5). By contrast, patient PTZ30 received a supratotal resection that removed l CE tumor and the area of infiltrated edema. This patient showed signs of tumor recurrence 27 month after surgery in the posterior area of the resection cavity (Fig. 5), being still alive at this point. These examples reinforce the notion that supratotal resection should include areas of vasogenic edemas, particularly those close to the CE tumor.

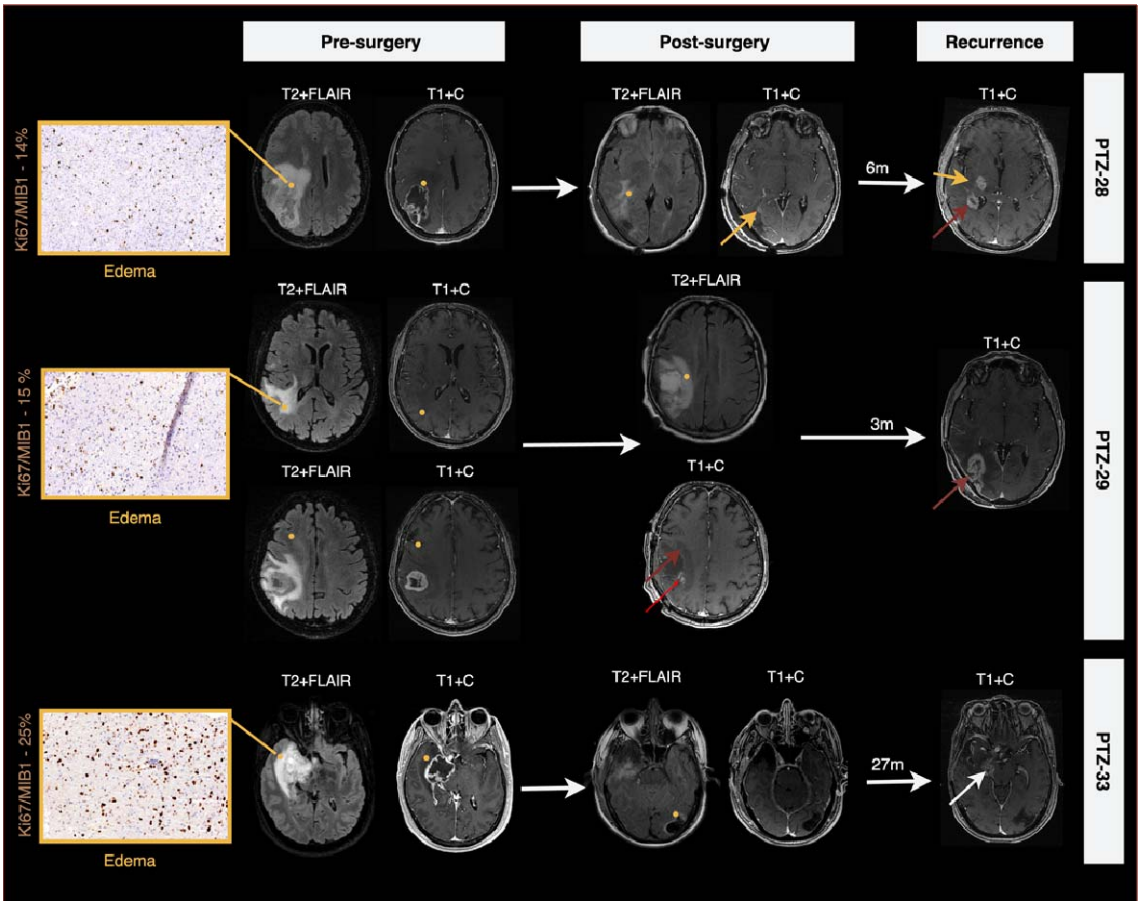

Figure 5. Tumor progression from infiltrated edema regions. MRI images (T1 sequence + contrast, T1+C; T2 FLAIR sequence, FLAIR) of three selected patients. The images were obtained before and after surgery, and at the time of tumor recurrence. The yellow dots indicate the location of the edema biopsies. Representative images of the immunohistochemical staining of these edema biopsies using the MIB1 antibody are shown on the left. In the post-surgical images, the brown arrow points towards regions of residual CE tumor in PTZ28 and PTZ29. In the MRI image at recurrence, the yellow arrow points towards CE tumor that appears at the location of the residual infiltrated edema in PTZ28 and PTZ29. In PTZ 28, the brown arrow points towards CE tumor that grew from the residual CE disease. In PTZ30, the white arrow points towards the location of the CE tumor that grew at the tumor cavity in the posterior region.

Prognosis value of the gene panel

We performed a correlation analysis between the expression of the different genes in our panel and the progression of the GB patients, which were separated in two groups based on the extent of resection. We focused on the edema and the CE samples as they were the ones with a higher sampling size. Among the edema biopsies, the expression of most of the genes had a higher

impact among the GTR patients, with some myeloid, astrocytic and oligodendrocyte genes showing a significant inverse correlation with overall survival (Fig. 6A). Among the CE biopsies, the impact of many genes was also higher among GTR patients, suggesting that the phenotype of the tumor core influences the nature of the infiltrative area. Higher level of expression of immune genes (myeloid and T cells), and also oligodendrocyte markers, were inversely correlated with the survival of the patients (Fig. 6A). Notably, although it was not statistically significant, the impact of the expression of immune genes showed a positive correlation with survival in patients receiving a non-complete resection of the CE tumor (Fig. 6A).

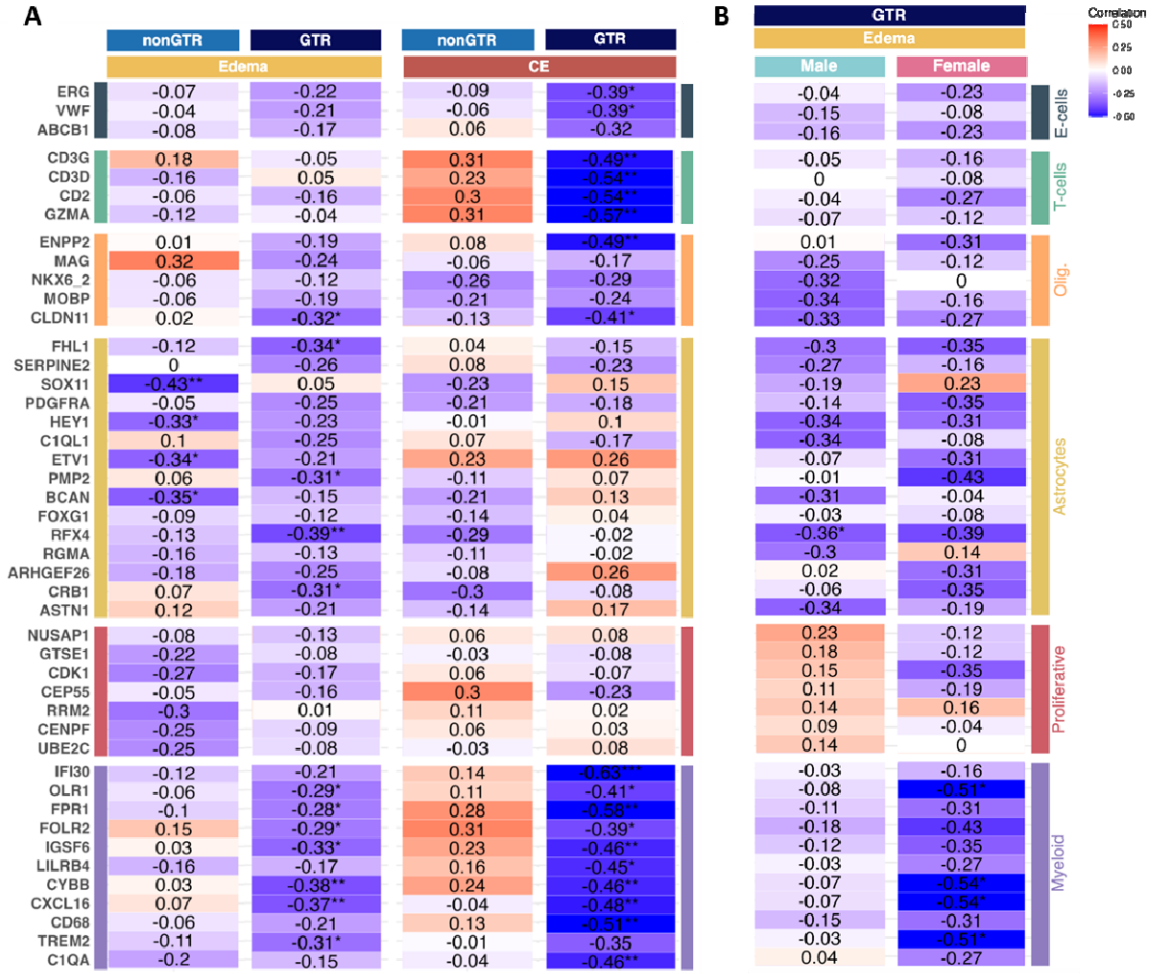

Figure 6. Association of specifc markers and their scores with survival. A) Heatmap showing the correlation between specific gene expresión and overall survival in edema and contrast-enhancing (CE) tumor regions. The simples were separated depending on the extent of the resection of the patient: Gross Total Resection (GTR) and non-GTR. Genes are grouped by cell type: Endothelial cells (E-cells), T-cells, Oligodendrocyte cells (Olig.), Astrocytes, Proliferative cells, and Myeloid cells. **B)** Heatmap showing the correlation between specific gene expression and overall survival in

edema regions from male and female patients that received GTR. * P≤0.05, ** P≤0.01, *** P≤0.001.

Considering the differences previously observed in the cellular phenotype of male and female patients (Fig. 3), we analyzed separately the impact of edema gene expression among the GTR group of patients. Notably, the expression of myeloid genes showed a strong inverse correlation with survival, but only in female patients, whereas in male patients, higher expression of proliferative genes seemed to correlate with better survival (although not significantly). These finding suggest that the TME and the degree of tumor infiltration in the peripheral zone of GB has a different impact on the progression of the disease depending on the sex of the patients.

Discussion

GB is one of the most challenging cancers to treat, with only a few successful clinical trials in the last decades. One of the approaches that has more significantly impacted the OS of GB is the improvement of surgical procedures, including the use of 5-ALA or RAMAN spectroscopy, to aid in GB margin delineation [3]. In addition, the extension of surgery to non-CE regions has been shown to significantly improve patient prognosis [5-7]. However, distinguishing non-CE tumor from edema, which is also characterized by high FLAIR signals, remains challenging and largely depends on subjective radiological criteria. Our IHC findings confirm the tumorigenic nature of the regions classified as non-CE tumor, and our gene panel analysis indicates that the cellular landscape of these areas is similar to that of the tumor core in most cases. However, the data also suggest the presence of tumorigenic features in areas of edema or even in radiologically normal regions, which has been suggested in the review of necropsies of GB patients [23]. These results suggest that there may be an additional benefit for some patients by extending the surgery beyond the CE and the non-CE tumor. Furthermore, these findings highlight the need for more reliable and reproducible MRI biomarkers (probably combining diffusion and perfusion weight imaging and spectroscopy) to predict the presence of residual tumor cells, hidden behind high FLAIR signals. [24-26].

Due to the small cohort size and the fact that many patients were still alive at the time of the analysis, we could not definitively confirm the benefit of supratotal resections. However, we observed a striking difference between patients in whom the entire CE tumor was resected (GTR) and those in whom residual CE tumor remained after surgery (non-GTR). A Norwegian group has

previously documented a significant superior benefit of complete CE resections compared to neartotal resections [27], suggesting that even small amounts of residual CE tumor may influence disease progression and/or treatment response. However, further research is necessary to validate these differences. In any case, the molecules and mechanisms that govern tumor growth in the core of GB tumors, which are the ones most commonly studied, are likely to be highly relevant in cases where some CE tumor remains. However, in patients receiving GTR, GB recurrence is caused by residual tumor cells infiltrating the brain parenchyma that are not exposed to the typical pressures of the core (e.g. hypoxia, necrosis, angiogenic signals). In the PBZ, for example, the interaction between GB cells and neurons is particularly relevant, as it contributes to their invasive and treatment-resistant properties [28-30]. Despite the logical underpinnings of this hypothesis, there is a paucity of clinical trials that have prospectively or retrospectively sought to categorize the response of GB patients to treatment based on the residual tumor volume. A seminal study by Ellingson et al. determined that postoperative residual CE tumor volume is an independent prognostic factor for standard chemoradiation, but also for bevacizumab [34]. Notably, the hazard ratio is particularly elevated for patients receiving vorinostat, a histone deacetylase inhibitor, with numerous long-term survivors in the group of patients with minimal residual CE tumor [34, 35]. Conversely, some immunotherapies appear to be more effective in cases where some CE tumor remains visible after surgery [36]. Consequently, we hypothesize that the vulnerabilities of core and infiltrative cells may be distinctly different, and that GB patients should be categorized based on the presence or absence of residual CE tumor, and treated accordingly as distinct diseases.

In a recent study, we established that neoplastic NKG2C expression could serve as a biomarker for immunotherapy response in GB patients, but only for those undergoing complete resection [13]. We showed that overexpressing NKG2C in a mouse GB model induced a shift in the immune microenvironment, characterized by a diminished immunosuppressive profile of macrophages. Furthermore, increased NKG2C expression in the PBZ compared to the tumor core was observed, which is consistent with the abundance of microglia with a reduced immunosuppressive environment described by other authors in the periphery of GB tumors [31-34]. The results presented here suggest that among patients receiving GTR, higher levels of myeloid-related markers and more reduced levels of T cell markers in the extra-tumoral biopsies are correlated with worse prognosis, suggesting that the amount and/or the type of immune cells present in the PBZ are responsible for the type of response to conventional chemo and radiotherapy. It will be

worthwhile to test in the future whether our gene panel has a predictive value for immunotherapies for GB patients and to confirm the relevance of the extent of resection in the response to this kind of treatment.

A number of discrepancies were identified in the histological parameters typically employed for the quantification of tumor infiltration. In our cohort, there was no clear correlation within the PBZ between the MIB1 proliferative index and the degree of cellularity. Moreover, we found gender and age-related disparities in their accumulation, with the former being more prevalent among female patients and older age groups. In relation to this, we found that myeloid markers accumulate with age in the peripheral area of older patients, but also in female vs male tumors. Thus, the high MIB1 staining could be due not only to tumor, but also stromal cells, such as macrophages, which have been shown to be activated and start proliferating in response to brain damage [35]. Indeed, proliferative markers selected in our gene set were also expressed in a cluster of macrophages (Fig. 3), and changes in the function of these cells have been linked to defects in injury repair in elderly subjects [36]. The incidence of GBM increases with age, a phenomenon attributed to the interplay between vascular, immune and senescent alterations that accumulate during the aging process, the so-called inflammaging [22, 37]. Corroborating this, age has been shown to be inversely correlated with clinical outcomes and is a strong prognostic factor for the course of most primary brain tumors, including GBM, although this finding is subject to controversy due to the less aggressive treatment that elderly patients typically receive [22, 38]. In the present cohort, we observed no significant differences in survival between young and elderly patients, irrespective of the extent of resection. However, our data suggest that the TME at the periphery might be very distinct in these two groups of patients. In relation to that, the worse prognosis of elderly GB patients, particularly in response to immunotherapies, has been recently attributed to molecular and cellular alterations in the extra-tumoral zone [39, 40]. Regarding sex differences, while the higher incidence of GBM in men is well-documented, little is known about potential brain and systemic differences between male and female patients or how these differences influence responses to specific treatments. Notably, macrophage function has been linked to sexual dimorphism in the inflammatory response to traumatic brain injury [35] and in GBM [36, 37]. Moreover, survival outcomes in males and females with GBM may be dependent on distinct mechanisms [38]. These findings suggest that micro- and macro-environmental changes occur in the brain in the presence of a GBM tumor, further influenced by age and sex. Further research is necessary to elucidate the complex network of myeloid cells and their functions within

the PBZ of gliomas, and the manner in which these cells influence tumor recurrence and treatment response in the different groups of patients.

A plethora of reasons have been posited to explain the dearth of success in GB clinical trials, including the fact that a significant proportion of the biological knowledge about this disease is based on studies performed on surgically-resected samples, which typically comprise the CE-region. We hope that our study helps to diminish that gap and provides tool to classify the heterogeneous nature of the GB tumor margin. However, we are aware that the relatively modest size of the patient cohort may constrain the prognostic significance of certain molecular and cellular markers examined. Another limitation is that the assessment of MGMT methylation status was not feasible in all cases. Nonetheless, the preliminary results suggest that the status of the MGMT promoter could be particularly relevant for GTR patients, a hypothesis that has been previously postulated by others [41]. Additional samples are being obtained to bolster the study's conclusions and to expand the investigation to identify biomarkers that might be applicable to specific tumor subtypes, particularly those observed in female patients. It is hoped that the gene expression panel will facilitate the expansion of the analysis to additional samples and patients, thereby providing a more comprehensive understanding of the cellular landscape of the peritumoral zone in relation with intra and inter-tumoral heterogeneity of GB.

References

[1] D.N. Louis, A. Perry, G. Reifenberger, A. von Deimling, D. Figarella-Branger, W.K. Cavenee, H. Ohgaki, O.D. Wiestler, P. Kleihues, D.W. Ellison, The 2016 World Health Organization Classification of Tumors of the Central Nervous System: a summary, Acta Neuropathol, 131 (2016) 803-820.
[2] M. Rapp, J. Baernreuther, B. Turowski, H.J. Steiger, M. Sabel, M.A. Kamp, Recurrence Pattern Analysis of Primary Glioblastoma, World Neurosurg, 103 (2017) 733-740.
[3] J.S. Young, R.A. Morshed, S.L. Hervey-Jumper, M.S. Berger, The surgical management of diffuse gliomas: Current state of neurosurgical management and future directions, Neuro Oncol, 25 (2023) 2117-2133.
[4] G. Broggi, R. Altieri, V. Barresi, F. Certo, G.M. Barbagallo, M. Zanelli, A. Palicelli, G. Magro, R. Caltabiano, Histologic Definition of Enhancing Core and FLAIR Hyperintensity Region of Glioblastoma, IDH-Wild Type: A Clinico-Pathologic Study on a Single-Institution Series, Brain Sciences, 2023.
[5] A.M. Molinaro, S. Hervey-Jumper, R.A. Morshed, J. Young, S.J. Han, P. Chunduru, Y. Zhang, J.J. Phillips, A. Shai, M. Lafontaine, J. Crane, A. Chandra, P. Flanigan, A. Jahangiri, G. Cioffi, Q. Ostrom, J.E. Anderson, C. Badve, J. Barnholtz-Sloan, A.E. Sloan, B.J. Erickson, P.A. Decker, M.L. Kosel, D. LaChance, J. Eckel-Passow, R. Jenkins, J. Villanueva-Meyer, T. Rice, M. Wrensch, J.K. Wiencke, N.A. Oberheim Bush, J. Taylor, N. Butowski, M. Prados, J. Clarke, S. Chang, E. Chang, M. Aghi, P. Theodosopoulos, M. McDermott, M.S. Berger, Association of Maximal Extent of Resection of Contrast-Enhanced and Non-Contrast-Enhanced Tumor With Survival Within Molecular Subgroups of Patients With Newly Diagnosed Glioblastoma, JAMA Oncol, 6 (2020) 495-503.
[6] Y.W. Park, K.S. Choi, M. Foltyn-Dumitru, G. Brugnara, R. Banan, S. Kim, K. Han, J.E. Park, T. Kessler, M. Bendszus, S. Krieg, W. Wick, F. Sahm, S.H. Choi, H.S. Kim, J.H. Chang, S.H. Kim, D. Wongsawaeng, J.M. Pollock, S.K. Lee, R.F. Barajas, Jr., P. Vollmuth, S.S. Ahn, Incorporating Supramaximal Resection into Survival Stratification of IDH-wildtype Glioblastoma: A Refined Multi-institutional Recursive Partitioning Analysis, Clin Cancer Res, 30 (2024) 4866-4875.
[7] P. Karschnia, J.S. Young, A. Dono, L. Hani, T. Sciortino, F. Bruno, S.T. Juenger, N. Teske, R.A. Morshed, A.F. Haddad, Y. Zhang, S. Stoecklein, M. Weller, M.A. Vogelbaum, J. Beck, N. Tandon, S. Hervey-Jumper, A.M. Molinaro, R. Ruda, L. Bello, O. Schnell, Y. Esquenazi, M.I. Ruge, S.J. Grau, M.S. Berger, S.M. Chang, M. van den Bent, J.C. Tonn, Prognostic validation of a new classification system for extent of resection in glioblastoma: A report of the RANO resect group, Neuro Oncol, 25 (2023) 940-954.
[8] J.K.W. Gerritsen, J.S. Young, S.M. Chang, S.M. Krieg, C. Jungk, M.J. van den Bent, D.D. Satoer, S. Ille, P. Schucht, B.V. Nahed, M.L.D. Broekman, M. Berger, S. De Vleeschouwer, A. Vincent, SUPRAMAX-study: supramaximal resection versus maximal resection for glioblastoma patients: study protocol for an international multicentre prospective cohort study (ENCRAM 2201), BMJ Open, 14 (2024) e082274.
[9] J.M. Lemee, A. Clavreul, P. Menei, Intratumoral heterogeneity in glioblastoma: don't forget the peritumoral brain zone, Neuro Oncol, 17 (2015) 1322-1332.
[10] T. Hide, Y. Komohara, Oligodendrocyte Progenitor Cells in the Tumor Microenvironment, Adv Exp Med Biol, 1234 (2020) 107-122.
[11] M. Giambra, A. Di Cristofori, S. Valtorta, R. Manfrellotti, V. Bigiogera, G. Basso, R.M. Moresco, C. Giussani, A. Bentivegna, The peritumoral brain zone in glioblastoma: where we are and where we are going, Journal of Neuroscience Research, 101 (2023) 199-216.
[12] A. Ballestín, D. Armocida, V. Ribecco, G. Seano, Peritumoral brain zone in glioblastoma: biological, clinical and mechanical features, Frontiers in Immunology, 15 (2024).

[13] O. de Dios, M.A. Ramírez-González, I. Gómez-Soria, B. Segura-Collar, J. Manosalva, D. Megías, C.E. De Andrea, L. Fernández-Rubio, A. Hernández-Laín, J.M. Sepúlveda-Sánchez, M.E. Rodriguez-Ruiz, Á. Pérez-Núñez, D.A. Wainwright, R. Gargini, P. Sánchez-Gómez, NKG2C/KLRC2 tumor cell expression enhances immunotherapeutic efficacy against glioblastoma, Journal for ImmunoTherapy of Cancer, 12 (2024) e009210.
[14] Y. Xie, L. He, R. Lugano, Y. Zhang, H. Cao, Q. He, M. Chao, B. Liu, Q. Cao, J. Wang, Y. Jiao, Y. Hu, L. Han, Y. Zhang, H. Huang, L. Uhrbom, C. Betsholtz, L. Wang, A. Dimberg, L. Zhang, Key molecular alterations in endothelial cells in human glioblastoma uncovered through single-cell RNA sequencing, JCI Insight, 6 (2021).
[15] M.J. Goldman, B. Craft, M. Hastie, K. Repečka, F. McDade, A. Kamath, A. Banerjee, Y. Luo, D. Rogers, A.N. Brooks, J. Zhu, D. Haussler, Visualizing and interpreting cancer genomics data via the Xena platform, Nature Biotechnology, 38 (2020) 675-678.
[16] M. Uhlen, C. Zhang, S. Lee, E. Sjostedt, L. Fagerberg, G. Bidkhori, R. Benfeitas, M. Arif, Z. Liu, F. Edfors, K. Sanli, K. von Feilitzen, P. Oksvold, E. Lundberg, S. Hober, P. Nilsson, J. Mattsson, J.M. Schwenk, H. Brunnstrom, B. Glimelius, T. Sjoblom, P.H. Edqvist, D. Djureinovic, P. Micke, C. Lindskog, A. Mardinoglu, F. Ponten, A pathology atlas of the human cancer transcriptome, Science, 357 (2017).
[17] D. Cantero, M. Mollejo, J.M. Sepulveda, N. D'Haene, M.J. Gutierrez-Guaman, A. Rodriguez de Lope, C. Fiano, J.S. Castresana, L. Lebrun, J.A. Rey, I. Salmon, B. Melendez, A. Hernandez-Lain, TP53, ATRX alterations, and low tumor mutation load feature IDH-wildtype giant cell glioblastoma despite exceptional ultra-mutated tumors, Neurooncol Adv, 2 (2020) vdz059.
[18] A.C. Yang, R.T. Vest, F. Kern, D.P. Lee, M. Agam, C.A. Maat, P.M. Losada, M.B. Chen, N. Schaum, N. Khoury, A. Toland, K. Calcuttawala, H. Shin, R. Palovics, A. Shin, E.Y. Wang, J. Luo, D. Gate, W.J. Schulz-Schaeffer, P. Chu, J.A. Siegenthaler, M.W. McNerney, A. Keller, T. Wyss-Coray, A human brain vascular atlas reveals diverse mediators of Alzheimer's risk, Nature, 603 (2022) 885-892.
[19] N. Abdelfattah, P. Kumar, C. Wang, J.S. Leu, W.F. Flynn, R. Gao, D.S. Baskin, K. Pichumani, O.B. Ijare, S.L. Wood, S.Z. Powell, D.L. Haviland, B.C. Parker Kerrigan, F.F. Lang, S.S. Prabhu, K.M. Huntoon, W. Jiang, B.Y.S. Kim, J. George, K. Yun, Single-cell analysis of human glioma and immune cells identifies S100A4 as an immunotherapy target, Nat Commun, 13 (2022) 767.
[20] X. Shao, J. Liao, X. Lu, R. Xue, N. Ai, X. Fan, scCATCH: Automatic Annotation on Cell Types of Clusters from Single-Cell RNA Sequencing Data, iScience, 23 (2020) 100882.
[21] Y. Mei, X. Wang, J. Zhang, D. Liu, J. He, C. Huang, J. Liao, Y. Wang, Y. Feng, H. Li, X. Liu, L. Chen, W. Yi, X. Chen, H.M. Bai, X. Wang, Y. Li, L. Wang, Z. Liang, X. Ren, L. Qiu, Y. Hui, Q. Zhang, Q. Leng, J. Chen, G. Jia, Siglec-9 acts as an immune-checkpoint molecule on macrophages in glioblastoma, restricting T-cell priming and immunotherapy response, Nat Cancer, 4 (2023) 1273-1291.
[22] M. Kim, E. Ladomersky, A. Mozny, M. Kocherginsky, K. O'Shea, Z.Z. Reinstein, L. Zhai, A. Bell, K.L. Lauing, L. Bollu, E. Rabin, K. Dixit, P. Kumthekar, L.C. Platanias, L. Hou, Y. Zheng, J. Wu, B. Zhang, M. Hrachova, S.A. Merrill, M.M. Mrugala, V.C. Prabhu, C. Horbinski, C.D. James, B. Yamini, Q.T. Ostrom, M.O. Johnson, D.A. Reardon, R.V. Lukas, D.A. Wainwright, Glioblastoma as an age-related neurological disorder in adults, Neurooncol Adv, 3 (2021) vdab125.
[23] T. Yamahara, Y. Numa, T. Oishi, T. Kawaguchi, T. Seno, A. Asai, K. Kawamoto, Morphological and flow cytometric analysis of cell infiltration in glioblastoma: a comparison of autopsy brain and neuroimaging, Brain Tumor Pathol, 27 (2010) 81-87.
[24] J. Juan-Albarracín, E. Fuster-Garcia, G.A. García-Ferrando, J.M. García-Gómez, ONCOhabitats: A system for glioblastoma heterogeneity assessment through MRI, International Journal of Medical Informatics, 128 (2019) 53-61.

[25] A. Elson, E. Paulson, J. Bovi, M. Siker, C. Schultz, P.S. Laviolette, Evaluation of pre-radiotherapy apparent diffusion coefficient (ADC): patterns of recurrence and survival outcomes analysis in patients treated for glioblastoma multiforme, Journal of Neuro-Oncology, 123 (2015) 179-188.
[26] A. Michalska-Foryszewska, M. Bujko, A. Kwiatkowska-Miernik, K. Ziemba, K. Sklinda, J. Walecki, B. Mruk, The peritumoral brain zone in glioblastoma: a review of the pretreatment approach, Pol J Radiol, 89 (2024) e480-e487.
[27] L.S. Bjorland, R. Mahesparan, Ø. Fluge, B. Gilje, K. Dæhli Kurz, E. Farbu, Impact of extent of resection on outcome from glioblastoma using the RANO resect group classification system: a retrospective, population-based cohort study, Neuro-Oncology Advances, 5 (2023) vdad126.
[28] M. Portela, V. Venkataramani, N. Fahey-Lozano, E. Seco, M. Losada-Perez, F. Winkler, S. Casas-Tinto, Glioblastoma cells vampirize WNT from neurons and trigger a JNK/MMP signaling loop that enhances glioblastoma progression and neurodegeneration, PLoS Biol, 17 (2019) e3000545.
[29] V. Venkataramani, Y. Yang, M.C. Schubert, E. Reyhan, S.K. Tetzlaff, N. Wissmann, M. Botz, S.J. Soyka, C.A. Beretta, R.L. Pramatarov, L. Fankhauser, L. Garofano, A. Freudenberg, J. Wagner, D.I. Tanev, M. Ratliff, R. Xie, T. Kessler, D.C. Hoffmann, L. Hai, Y. Dorflinger, S. Hoppe, Y.A. Yabo, A. Golebiewska, S.P. Niclou, F. Sahm, A. Lasorella, M. Slowik, L. Doring, A. Iavarone, W. Wick, T. Kuner, F. Winkler, Glioblastoma hijacks neuronal mechanisms for brain invasion, Cell, 185 (2022) 2899-2917 e2831.
[30] F. Winkler, H.S. Venkatesh, M. Amit, T. Batchelor, I.E. Demir, B. Deneen, D.H. Gutmann, S. Hervey-Jumper, T. Kuner, D. Mabbott, M. Platten, A. Rolls, E.K. Sloan, T.C. Wang, W. Wick, V. Venkataramani, M. Monje, Cancer neuroscience: State of the field, emerging directions, Cell, 186 (2023) 1689-1707.
[31] S. Darmanis, S.A. Sloan, D. Croote, M. Mignardi, S. Chernikova, P. Samghababi, Y. Zhang, N. Neff, M. Kowarsky, C. Caneda, G. Li, S.D. Chang, I.D. Connolly, Y. Li, B.A. Barres, M.H. Gephart, S.R. Quake, Single-Cell RNA-Seq Analysis of Infiltrating Neoplastic Cells at the Migrating Front of Human Glioblastoma, Cell Reports, 21 (2017) 1399-1410.
[32] Z. Chen, X. Feng, C.J. Herting, V.A. Garcia, K. Nie, W.W. Pong, R. Rasmussen, B. Dwivedi, S. Seby, S.A. Wolf, D.H. Gutmann, D. Hambardzumyan, Cellular and Molecular Identity of Tumor-Associated Macrophages in Glioblastoma, Cancer Research, 77 (2017) 2266-2278.
[33] R. Tamura, K. Ohara, H. Sasaki, Y. Morimoto, K. Kosugi, K. Yoshida, M. Toda, Difference in Immunosuppressive Cells Between Peritumoral Area and Tumor Core in Glioblastoma, World Neurosurg, 120 (2018) e601-e610.
[34] H. Rahimi Koshkaki, S. Minasi, A. Ugolini, G. Trevisi, C. Napoletano, I.G. Zizzari, M. Gessi, F. Giangaspero, A. Mangiola, M. Nuti, F.R. Buttarelli, A. Rughetti, Immunohistochemical Characterization of Immune Infiltrate in Tumor Microenvironment of Glioblastoma, Journal of Personalized Medicine, 2020.
[35] R. Hausmann, P. Betz, The course of MIB-1 expression by cerebral macrophages following human brain injury, Leg Med (Tokyo), 4 (2002) 79-83.
[36] L. Duong, H.G. Radley, B. Lee, D.E. Dye, F.J. Pixley, M.D. Grounds, D.J. Nelson, C. Jackaman, Macrophage function in the elderly and impact on injury repair and cancer, Immunity & Ageing, 18 (2021) 4.
[37] B. Segura-Collar, P. Mata-Martinez, A. Hernandez-Lain, P. Sanchez-Gomez, R. Gargini, Blood-Brain Barrier Disruption: A Common Driver of Central Nervous System Diseases, Neuroscientist, 28 (2022) 222-237.
[38] A. Wick, T. Kessler, A.E.H. Elia, F. Winkler, T.T. Batchelor, M. Platten, W. Wick, Glioblastoma in elderly patients: solid conclusions built on shifting sand?, Neuro-Oncology, 20 (2018) 174-183.
[39] M.A.-O.X. Johnson, A.A.-O. Bell, K.A.-O. Lauing, E.A.-O. Ladomersky, L.A.-O. Zhai, M.A.-O. Penco-Campillo, Y.A.-O. Shah, E.A.-O. Mauer, J.A.-O. Xiu, T.A.-O. Nicolaides, M.A.-O. Drumm, K.A.-

O.X. McCortney, O.A.-O. Elemento, M.A.-O. Kim, P.A.-O. Bommi, J.A.-O. Low, R.A.-O. Memon, J.A.-O.X. Wu, J.A.-O. Zhao, X.A.-O. Mi, M.A.-O. Glantz, S.A.-O. Sengupta, B.A.-O. Castro, B.A.-O. Yamini, C.A.-O. Horbinski, D.A.-O. Baker, T.A.-O. Walunas, G.A.-O. Schiltz, R.A.-O. Lukas, D.A.-O. Wainwright, Advanced Age in Humans and Mouse Models of Glioblastoma Show Decreased Survival from Extratumoral Influence.
[40] E. Ladomersky, L. Zhai, K.L. Lauing, A. Bell, J. Xu, M. Kocherginsky, B. Zhang, J.D. Wu, J.R. Podojil, L.C. Platanias, A.Y. Mochizuki, R.M. Prins, P. Kumthekar, J.J. Raizer, K. Dixit, R.V. Lukas, C. Horbinski, M. Wei, C. Zhou, G. Pawelec, J. Campisi, U. Grohmann, G.C. Prendergast, D.H. Munn, D.A. Wainwright, Advanced Age Increases Immunosuppression in the Brain and Decreases Immunotherapeutic Efficacy in Subjects with Glioblastoma, Clin Cancer Res, 26 (2020) 5232-5245.
[41] F. Incekara, M. Smits, S.R. van der Voort, H.J. Dubbink, P.N. Atmodimedjo, J.M. Kros, A.J.P.E. Vincent, M. van den Bent, The Association Between the Extent of Glioblastoma Resection and Survival in Light of MGMT Promoter Methylation in 326 Patients With Newly Diagnosed IDH-Wildtype Glioblastoma, Frontiers in Oncology, 10 (2020).